Robust surface functionalization of PDMS through atmospheric pressure atomic layer deposition

Santoso, A.; van den Berg, B.J.; Saedy, S.; Goodwin, Eden ; van Steijn, V.; van Ommen, J.R.

Important note
To cite this publication, please use the final published version (if applicable).
Please check the document version above.

ATOMIC LAYER DEPOSITION

INTERNATIONAL JOURNAL

Research Article

Robust surface functionalization of PDMS through atmospheric pressure atomic layer deposition

Albert Santoso[1], Bart J. van den Berg[1], Saeed Saedy[1], Eden Goodwin[2], Volkert van Steijn[1], J. Ruud van Ommen[1]

1   Department of Chemical Engineering, Delft University of Technology, 2624HZ, Delft, The Netherlands
2   Department of Chemistry, Carleton University, Ottawa, K1S 5B6, Canada
Corresponding author: J. Ruud van Ommen (*j.r.vanommen@tudelft.nl*)

Abstract

Polydimethylsiloxane (PDMS) has been widely employed as a material for microreactors and lab-on-a-chip devices. However, in its applications, PDMS suffers from two major problems: its weak resistance against common organic solvents and its chemically non-functional surface. To overcome both issues, atmospheric pressure atomic layer deposition (AP-ALD) can be used to deposit an inorganic nanolayer (TiO_x) on PDMS that, in turn, can be further functionalized. The inorganic nano layer is previously communicated to durably increase the organic solvent resistance of PDMS. In this study, we investigate the possibility of this TiO_x nano layer providing surface anchoring groups on PDMS surfaces, enabling further functionalization. We treat PDMS samples cured at three different temperatures with AP-ALD and measure the hydrophilicity of the treated samples as an indicator of the presence of surface anchoring groups. We find that all the treated PDMS samples become hydrophilic right after the AP-ALD treatment. We further find that the AP-ALD-treated PDMS samples cured at 150 °C and 200 °C maintain their hydrophilicity, while the samples cured at 70 °C become less hydrophilic over time. The presence of surface anchoring groups through TiO_x nano layer deposition on PDMS is further demonstrated and utilized by depositing gold nanoparticles (AuNPs) on the AP-ALD-treated samples. The samples exhibit visible light absorbance at 530 nm, a typical absorbance peak for AuNPs. In conclusion, this study demonstrates the use of nano layers grown by AP-ALD to solve the two major problems of PDMS simultaneously, widening its applicability, especially for use in high-end applications such as catalysis and bio-sensing.

Key words: PDMS, Atmospheric ALD, Titanium dioxide, wettability, functionalization

1. Introduction

In the fields of medicine, biology, and chemistry, there is a rising trend of using polydimethylsiloxane (PDMS) as a material for microfluidics and protective coatings [1, 2]. The high transparency, excellent biocompatibility, ease of rapid prototyping, and tunable bulk properties of PDMS make it an attractive

substrate, enabling wide selections of optical-based micro-(bio)processing [1, 3, 4]. However, PDMS has two major issues: its weak resistance against organic solvents and its chemically non-functional surface. When it comes in contact with common organic solvents such as chloroform and acetone, PDMS swells and deforms. Furthermore, the PDMS surface is naturally hydrophobic and mostly dominated by methyl groups, making it difficult to introduce functional groups such as hydroxyl, thiol, amine, carboxylic, epoxy rings, and many others [5, 6]. As a result, the use of PDMS is limited, especially in applications where the presence of functional groups or the use of organic solvents is vital [3, 4, 7, 8].

To overcome the limitations of PDMS, researchers explored two main directions: bulk modification and surface treatment [5, 9]. Since bulk modification leads to undesirable changes in PDMS bulk properties (e.g. softer/stiffer, lower transparency), wet and dry surface treatments have been explored [1, 4, 5, 10, 11]. A common dry surface treatment is the use of oxygen plasma to introduce hydroxyl groups on PDMS. While it renders the surface hydrophilic, the surface recovers to its initial hydrophobic state within hours known as hydrophobic recovery [12, 13]. Furthermore, this treatment does not render the surface inert such that oxygen-treated PDMS samples cannot be used for systems involving organic solvents. As such, numerous modifications involving liquid chemistry and sol-gel methods have been developed [14−19]. While using (hydroxyethyl)methacrylate (HEMA), polyethylene glycol (PEG), polyvinylpyrollidone (PVP), or polyvinyl alcohol (PVA) solutions to coat the PDMS surface does make the surface more hydrophilic [14−17], the introduced functional group could be desorbed and washed away by many solvents [15]. Furthermore, the PDMS is still susceptible to organic solvents. As an alternative, researchers looked into depositing non-organic layers. Roman and Culbertson used transition metal sol-gel precursors to introduce metal oxide groups [16], while the group of Weitz used tetraethyl orthosilicate (TEOS) and methyltrimethoxysilane (MTES) to deposit a glass-like substance on the PDMS surface [19]. While both offer a more robust layer to both protect the PDMS from direct organic solvent exposure and provide hydrophilic surface groups, the sol-gel method cannot be used to coat complex structures uniformly because the removal of the thick sol-gel solution using gas leaves unwanted residues. Apart from being uneven, the microscopically thick coating may compromise the bulk properties [20]. Therefore, vapor deposition of inorganic nanoscopically thin layers on PDMS becomes promising due to the use of a single phase in its whole deposition process while solving both issues of PDMS simultaneously [6, 21−26].

Among all vapor deposition methods, atomic layer deposition is renowned as it faithfully coats complex nanostructures with a wide variety of coating materials properties [27]. Using alternating reactions, the thickness of the coating layer, and its corresponding prop-erties [27], can be controlled in a straightforward manner. When it comes to polymeric substrates including the elastomer PDMS, substrate infiltration could occur [26, 28, 29]. Therefore, numerous terms have been coined to better represent the process, such as multiple pulsed infiltration, vapor phase infiltration, sequential infiltration synthesis, atomic layer deposition, or atomic layer infiltration [30]. The group of Parsons made use of this by exposing PDMS to a metal precursor pulse, then a water precursor pulse, for several hours before conducting a sequential atomic layer deposition, and a sequential molecular layer deposition resulting in a significantly lowered hydrophobic recovery rate for 200 h [6]. In their work, the surface growth and the subsurface growth were achieved in several process steps, and the samples' surface terminated with an organic-inorganic molecular layer (alucone) [6]. By contrast, our previous study communicated that both surface growth and subsurface infiltration of metal oxide occurs during atmospheric pressure deposition [31]. There, we showed that this unique surface-subsurface deposition contributes positively to increasing PDMS organic solvent resistance through a coating of titanium oxide [31]. Due to more than one phenomenon taking place in our previous and current work, we opt to use the more general term atomic layer deposition (ALD).

In this paper, we follow up on our previous work by extending the use of the atmospheric pressure ALD (AP-ALD) of titanium oxide (TiO_x) to functionalize the PDMS substrate. While TiO_x has been demonstrated to provide a protective layer against organic solvents [31], it also has potential in providing hydroxyl groups that act as anchoring points for other molecules or particles [17, 32, 33]. In this study, we measure the hydrophilicity of the treated samples as an indicator for the functionality. We
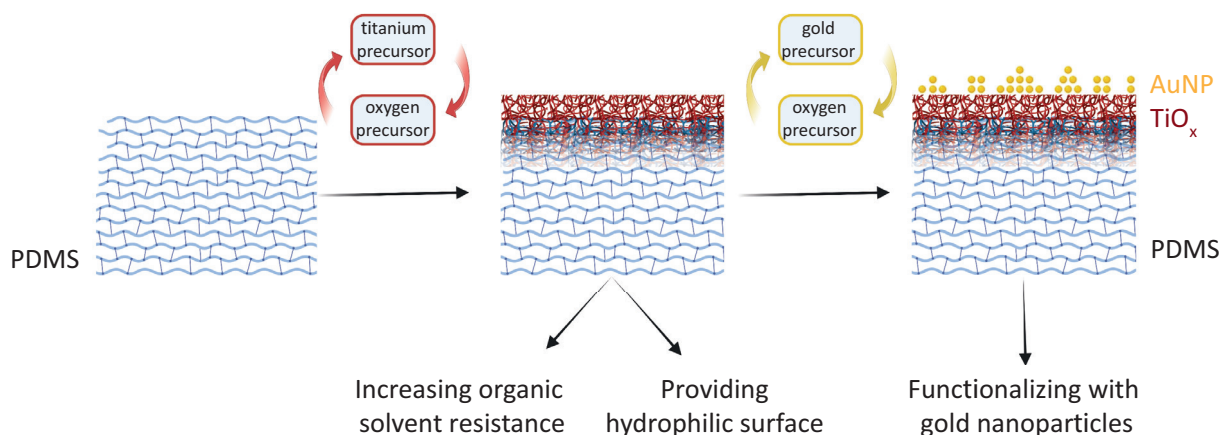
Figure 1. Illustration of modification of PDMS through deposition of a TiO_x nano layer and further functionalization through the deposition of gold nanoparticles (AuNPs). The deposition of a TiO_x nano layer both increases the organic solvent resistance of PDMS and renders the surface hydrophilic through hydroxyl groups. These groups act as anchoring points for further functionalization, here shown for AuNPs.

further demonstrate the presence of surface anchoring groups by functionalizing the treated PDMS surface by depositing gold nanoparticles (AuNPs) on top of the TiO_x layer, as illustrated in Figure 1. The presented results show a promising use of AP-ALD to tackle both weaknesses of PDMS in one go by increasing the organic solvent resistance and functionalizing the surface robustly while eliminating the need for expensive vacuum technology in its fabrication.

2. Method

2.1. Substrate preparation

PDMS samples were fabricated by mixing the elastomer and curing agent (Sylgard 184 Elastomer Kit, Dow Corning) in a ratio of 10:1. After manual stirring of the mixture for 2 min, trapped air bubbles were removed using a vacuum desiccator for 30 min. The degassed mixture was poured into a Petri dish and placed in the vacuum desiccator again for another 30 min. PDMS was then cured in an oven at 70 °C, 150 °C, or 200 °C for at least 10 hours. Samples of 25 mm × 30 mm (0.5 mm thick) were cut from the cured PDMS and bonded on a glass slide after plasma treatment (oxygen in air, Harrick, PDC-002) at 0.2–0.4 mbar for 140 s.

2.2. Atomic layer deposition of TiO_x layers

TiO_x was deposited using a home-built atmospheric-pressure setup with a tubular flat-substrate reactor, where the precursor was delivered parallel to the substrate, as described previously [31]. Tetrakis-dimethylamino titanium (IV) (TDMAT, >99.99% Merck Sigma) and ozone-enriched air (Sander Certizon) were used as titanium and oxygen precursor respectively, while nitrogen (N_2 99.999%, Linde) was used as carrier gas. The carrier gas flowed through a bubbler for the metal precursor (kept at 70 °C) at 0.5 L/min for 10 s, while the ozone-enriched air flowed at 0.7 L/min for 30 s. In between, the nitrogen purging was done at 2 L/min for 100 s. Unless otherwise stated, we performed 100 cycles and kept the chamber at 100 °C. The ALD temperature was chosen to avoid condensation of ALD precursors at too low a temperature and possible cracks due to thermal expansion and contraction of PDMS at too high a temperature during the deposition process. As a comparison to AP-ALD treatment, we also conducted TiO_x deposition through thermal atomic layer deposition (Th-ALD) and plasma enhanced atomic layer deposition (PE-ALD) in a commercial atomic layer deposition reactor (Veeco Fiji G2) at 10^{-5} mbar and 100 °C. While TDMAT was used as the Ti precursor, water and oxygen plasma were used for the oxygen precur-

sor in Th-ALD and PE-ALD, respectively. Both precursors were introduced into the chamber at 0.02 L/min for 60 ms alternatingly with 45 s (Th-ALD) or 5 s (PE-ALD) of nitrogen purging done in between. To ensure a fair comparison, we performed 100 cycles at 100 °C.

2.3. Atomic layer deposition of gold nanoparticles on TiO$_x$ layers

To demonstrate the ability to functionalize the TiO$_x$-treated PDMS surface, we performed a second AP-ALD treatment in which we deposited gold nanoparticles (AuNPs) on TiO$_x$-treated PDMS samples cured at 150 °C. AuNPs were deposited using trimethylphosphino-trimethyl gold(III) (6-Me, prepared according to literature procedure [34, 35]) and ozone-enriched air as a precursor for 5 cycles at 100 °C using the same ALD set-up. The nitrogen carrier gas flowed through a bubbler for the metal precursor (kept at 75 °C) at 0.5 L/min for 15 s, while the ozone-enriched air flowed at 0.7 L/min for 30 s. In between, the purging was done at 2 L/min for 100 s. As a control, we also deposited AuNPs on bare PDMS samples with similar operating parameters.

2.4. Surface characterization of AP-ALD-treated PDMS samples

In order to characterize the surface morphology, field emission scanning electron microscopy (FE-SEM, Hitachi Regulus SU8230) at a beam current of 1−5 µA and electron energy of 1−10 keV was conducted. To obtain the surface elemental information, X-ray photoelectron spectroscopy (XPS) (ThermoFisher Scientific Nexsa) equipped with a monochromatic Al Kα radiation source and a pass energy of 30 and 100 eV for the survey scan and ion-beam etching unit was used. Depth profiling was conducted by etching the surface using Ar+ ions (2 keV with a raster size of 2 mm) while a flood gun was used to compensate for the differential charging. Thermo Avantage 5.913 and CASA-XPS software were used to post-process the XPS peak profile, where the spectra were charge-corrected with the adventitious carbon peak at 284.8 eV. The thickness of the TiO$_x$ layer was approximated using an etch rate obtained in our previous study [31]. This thickness was used to calibrate the etch rate of the TiO$_x$ layer on PDMS during XPS measurements, indicating an approximated elemental depth profile.

2.5. Particle size distribution of the deposited AuNPs

To obtain the particle size distribution of AuNPs, ALD-coated PDMS samples were sonicated in HNO$_3$ 1 M (Merck Sigma) for 15 min and left immersed for 48 h to dissolve the TiO$_x$ layer under the AuNPs and disperse them into the solution. The solution was then centrifuged (MicroCL 21/21R, Thermoscientific) at 14800 rpm for 10 min and the supernatant was decanted as much as possible prior to being washed three times with ethanol (96%) and transferred onto Quantifoil copper TEM grids (coated with carbon). Transmission electron microscopy (TEM) images of the AuNPs were acquired using a JEOL JEM1400 microscope operating at a voltage of 120 kV working in bright-field mode. The average particle size and particle size distribution curves were obtained using the diameter of more than 350 individual particles analyzed using ImageJ.

2.6 Wettability study of TiO$_x$-coated PDMS samples

To quantify the surface wetting property, the dynamic contact angles were measured using a Krüss drop shape analyzer (Suppl. material 1: fig. S1) at ambient conditions. An automated dispensing system was used to form the droplet and to increase and decrease the volume of the droplet. After forming a droplet of milliQ-water at a needle and bringing it in close contact with the surface of a PDMS sample, the droplet formed a contact line with the surface. As the droplet's volume increased gradually, the droplet inflated while the contact line remained pinned, resulting in an increase in the contact angle. The maximum contact angle before the droplet unpinned and started advancing is referred to as the advancing

contact angle (θ_{adv}, Suppl. material 1: fig. S1a), After that, the volume of the droplet was decreased, resulting in again pinning of the contact line and a decrease in contact angle. The minimum contact angle before the droplet unpinned and started receding is referred to as the receding contact angle (θ_{rec}, Suppl. material 1: fig. S1b). Contact angle measurements were done every few minutes, 24 h, 48 h, 200 h, 400 h, and 800 h after the samples were taken out of the ALD reactors, with samples being stored in a glove box to reduce random air contamination during storage. Drop shape analysis software was used to measure contact angles from camera images. Average values were reported from 10 measurements via the typical uncertainty (2 s.d.).

2.7. Washing of the PDMS samples and ATR-FTIR characterization

To examine our hypothesis about the presence of uncured monomer in PDMS that diffuses out and compromises the AP-ALD coating, we pre-washed the PDMS samples to remove non-crosslinked molecules from the PDMS [36]. The PDMS samples were soaked in 70 mL cyclohexane (99% vol, Merck Sigma) for 72 h. Hereafter, the washing solvent was taken out and kept for infrared spectroscopy measurement, and a second soaking step of the PDMS samples was conducted for 24 h. After measuring the weight of the swollen PDMS samples, the samples were dried at room temperature for at least 8 h. The dried PDMS samples were weighed again to calculate the weight loss during the washing. The ATR-FTIR (attenuated total reflectance Fourier-transform infra-red spectroscopy) measurements on the washing solvents were performed on a Thermo Nicolet NEXUS instrument equipped with a liquid nitrogen cooled MCT detector with a wavelength range of 4000 to 500 cm^{-1}.

2.8. UV-Vis spectrophotometry study

To measure the photonic effect of the TiO$_x$-treated PDMS surface functionalized with AuNPs, light absorption was measured with a wide scan reading (300–800 nm) using a NanoDrop™ 2000/2000c spectrophotometer. The reported value was an average of 3 measurements via the typical uncertainty (2 s.d.).

3. Result and discussion

3.1. Simultaneous surface and subsurface growth in AP-ALD

Before examining the treated samples, we point out that deposition of TiO$_x$ on PDMS may result in both surface and subsurface growth, and therefore is more ambiguous to characterize [31]. Figure 2a shows the relative atomic percentage of titanium changes along the depth of the PDMS samples obtained using XPS depth profiling, while Figure 2b shows the corresponding XPS surface composition. On all samples, a significant percentage of Ti is observed on the surface, even to an etch depth of about 70–80 nm, indicating the formation of the TiO$_x$ layer. A closer look at Figure 2b confirms that the atomic ratio of titanium to oxygen is about 1 to 2, indicating TiO$_2$ deposition. The titanium atomic percentage of all samples gradually declines in a comparable manner along the etch depth, before dropping to a percentage of ~5% at the depth of 200 nm. This gradual decline indicates the formation of an infiltrated layer. This result is in good agreement with previous results [31]. For all three AP-ALD samples, we observe similar profiles, indicating that the curing temperature has no effect on the resulting surface-subsurface structure. This is expected because the average size of the pores in PDMS is in the range of a few tens of nm to a few μm [37], much larger than the size of the precursor molecules. Thus, irrespective of the relative difference between the pore sizes due to differences in crosslinking densities, the penetration behavior of the precursor is the same in all three samples. Additionally, we study the effect of the number of cycles on the depth profile. We find that the Ti2p signal is not detected on the samples deposited with
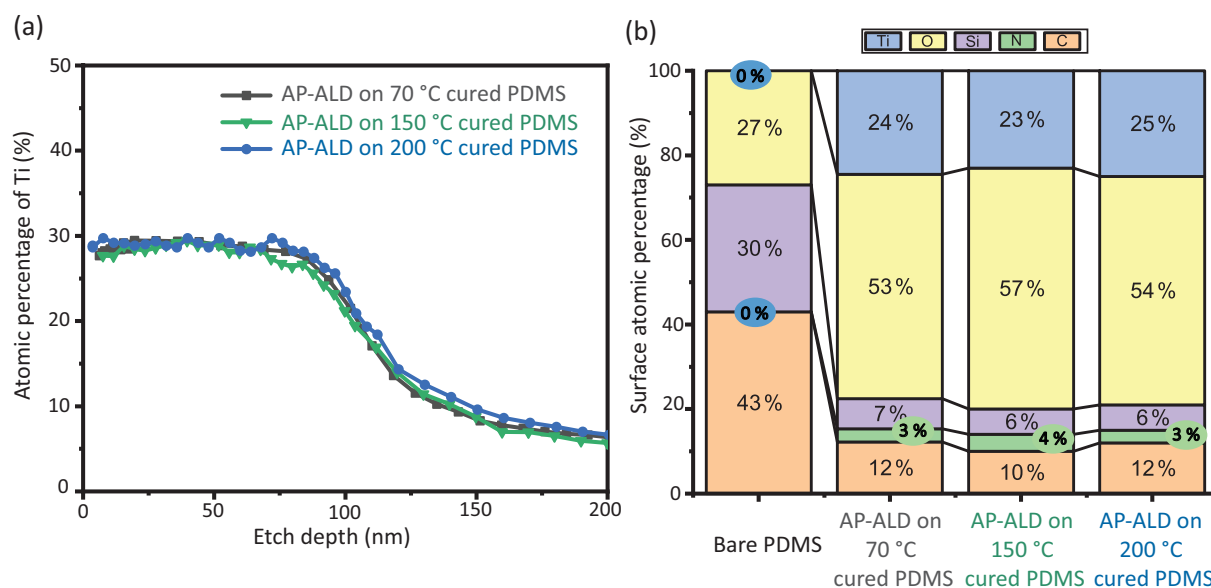
Figure 2. (**a**) XPS depth profiling showing the relative atomic percentage of titanium in the surface and subsurface of AP-ALD-coated PDMS samples cured at 70 °C, 150 °C, 200 °C, and (**b**) XPS elemental analysis of the surface.

10 cycles, while an appreciable signal is detected after 20 cycles (Suppl. material 1: fig. S2a), indicating the presence of nucleation delay, which is typical for non-reactive substrates such as PDMS [24, 26, 31].

Of note, XPS milling may influence the XPS reading. In case this artifact is significant, we expect it to influence the profiles obtained for different numbers of cycles in a similar way. Yet, when inspecting, for example, the profiles obtained with 50 and 100 cycles in Suppl. material 1: fig. S2b, we see that the minimum and maximum percentage is the same, while the gradient of the slope of these profiles differs significantly. We suspect that at the given number of cycles, the diffusion coefficient of the ALD precursors is not much reduced due to the wide range of PDMS pore sizes and that the fresh PDMS surface group at the end of the coated area reacts with the ALD precursors as well. We hence conclude that a higher number of ALD cycles leads to both a thicker TiO_x layer and a more moderate, deeper infiltration. We also note that this growth profile differs from commonly reported growth in vacuum ALD. Besides the XPS analysis of the surface and subsurface, an analysis of the surface by FE-SEM shows that the coating is visually smooth without nano cracks, even after 800 h, indicating a stable TiO_x layer (Suppl. material 1: fig. S3).

3.2. Hydrophilicity as indicator of functional surface

We use hydrophilicity as an indicator for the presence of surface anchoring groups (in this case hydroxyl groups) on the ALD-coated PDMS surfaces. More specifically, we use the contact angle of a droplet of water brought into contact with the coated surfaces. Although the observed angle depends on the way of contacting, it is bounded by the contact angle hysteresis range, with an upper and lower bound intrinsic to the surface. The upper bound, called the advancing contact angle, is taken as the relevant characteristic in this work. While the range is known to depend on the roughness of the surfaces, we confirm the roughness of the samples' surfaces to be similar [31]. The advancing contact angle (θ_{adv}) measurement of bare PDMS and AP-ALD-coated PDMS samples cured at different temperatures are presented in Figure 3a. Directly after coating ($t = 0$), the (three) bare PDMS samples show a similar advancing contact angle at 118°±1°, in accordance with reported values [38, 39]. The AP-ALD-coated PDMS samples exhibit a significantly lower θ_{adv}, around 68°±4° at $t = 0$. A closer look at the XPS surface composition of these samples shows a high TiO_x coverage (Figure 2b), indicating that the hydrophilicity of the samples depends on the composition and possibly on the structure of the TiO_x coating. To confirm, we conducted two additional types of ALD treatment on PDMS samples,

plasma enhanced ALD (PE-ALD) and thermal ALD (Th-ALD), that are known to yield notably different TiO$_x$ layers [31]: PE-ALD leads to a TiO$_x$ layer on top of the PDMS surface, while Th-ALD leads to a TiO$_x$ layer inside the PDMS (infilling). As expected, the PE-ALD-coated PDMS samples exhibit a θ$_{adv}$ of 69°±1° that is comparable to the AP-ALD-coated PDMS samples (Suppl. material 1: fig. S4a). This result is in line with the previous finding by Pessoa [23]. By contrast, the Th-ALD-coated PDMS samples exhibit a θ$_{adv}$ of 111°±2° that is comparable to bare PDMS samples (Suppl. material 1: fig. S4a). When looking at the surface elemental composition (Suppl. material 1: fig. S4b), the XPS surface spectra of PE-ALD-, Th-ALD-, and AP-ALD-coated PDMS samples show the expected profile of the TiO$_x$ layers [31]. Both PE-ALD- and AP-ALD-coated samples show a dominance of Ti2p peak with little C1s and Si2p peaks, indicating a high coverage of TiO$_x$ layers. By contrast, the Th-ALD-coated samples show a dominance of C1s and Si2p peaks with little Ti2p peaks, typical elements found in PDMS molecular chains. These XPS results are in line with previously reported SEM photos and XPS profiles [31]. These observations underline the importance of the type of TiO$_x$ layer, and the type of ALD treatment used, on the hydrophilicity of the coated PDMS samples.

A well-known phenomenon in the coating of PDMS samples is the gradual temporal change in surface composition leading to the recovery of the hydrophobicity [22]. To test the robustness of the AP-ALD treatment, we measured the advancing contact angle on the same samples over prolonged periods of time. While the hydrophobicity of the bare PDMS samples is constant in time, we find that θ$_{adv}$ of AP-ALD-coated PDMS samples cured at 70 °C increases along the duration of the measurement, reaching 89°±4° after 800 h (Figure 3a). This increase is significantly lower when compared to PE-ALD-coated PDMS samples cured at 70 °C (reaching 103°±1° after 800 h, see Suppl. material 1: fig. S4). We argue that the combined surface-subsurface TiO$_x$ layer obtained through AP-ALD acts as a barrier for the out-diffusion of uncured monomers, slowing down the hydrophobic recovery as compared to the surface-only TiO$_x$ layer obtained through PE-ALD. This is in line with the observation that the surface-subsurface TiO$_x$ layer obtained through AP-ALD shows no visual cracks (Suppl. material 1: fig. S3), while nano cracks have been reported in the surface-only TiO$_x$ layer obtained through PE-ALD [31]. While these nano cracks do not affect the hydrophilicity of the PE-ALD-coated samples at t = 0 (Suppl. material 1: fig. S4a), it becomes a route for the uncured monomers to out diffuse, leading to hydrophobic recovery after 800 h.

The AP-ALD coating on PDMS samples cured at 70 °C renders the surface hydrophilic over prolonged times, yet it is subject to change due to the out-diffusion of uncured monomers. Earlier studies have
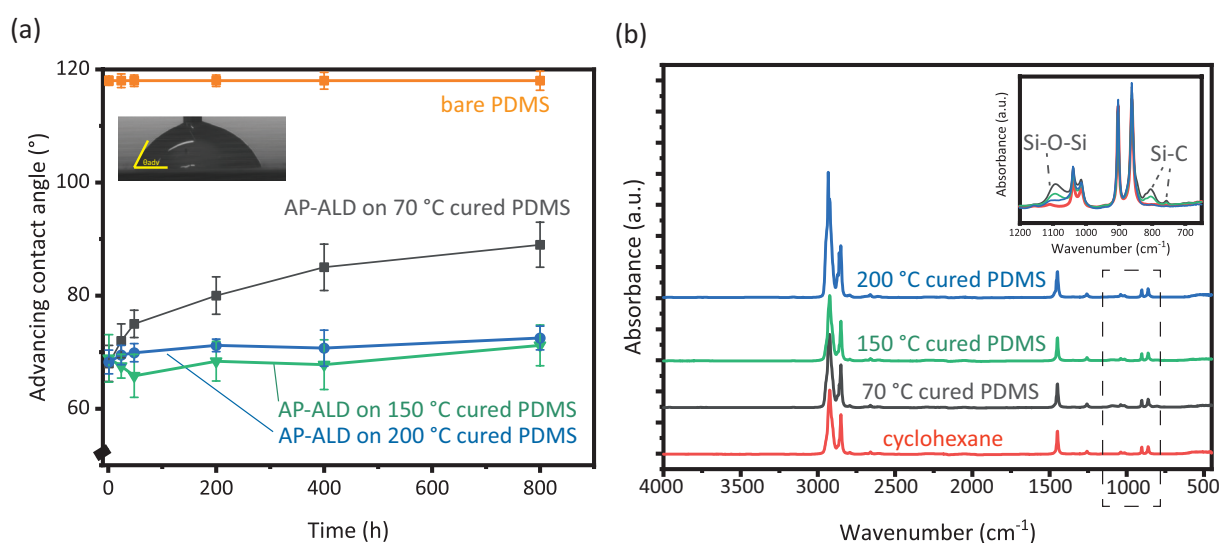

Figure 3. (**a**) Advancing contact angle measurement on bare and AP-ALD-coated PDMS samples cured at three different temperatures and (**b**) ATR-FTIR spectra of the solvent (cyclohexane) used to wash PDMS samples cured at different temperatures together with a control (pure cyclohexane).

suggested that curing of PDMS at higher temperatures changes the internal crosslinking of PDMS, leading to a tighter network [40] and fewer low-molecular-weight molecules [41]. For the AP-ALD-coated PDMS samples cured at 150 °C and 200 °C, we indeed observe a negligible increase of advancing contact angle, from 69°±4° after coating to 71°±4° after 800 h for 150 °C, and from 68°±2° after coating to 73°±2° after 800 h for 200 °C (Figure 3a). Another way to reduce the amount of uncured monomer present in PDMS samples is to wash the cured PDMS samples using a solvent. The ATR-FTIR spectra of the solvent used to wash PDMS samples cured at 70 °C, 150 °C, and 200 °C show elevated peaks associated with the Si-O-Si and Si-C bonds in reference to the spectrum of the pure solvent [6, 22, 42], with the amount of uncured monomer decreasing with increasing curing temperature (Figure 3b). As expected, the advancing contact angle of the AP-ALD-coated PDMS samples cured at 70 °C and washed prior to ALD show a reduction in hydrophobic recovery, reaching 80°±4° after 800 h. Given that the surface of the AP-ALD-coated PDMS samples cured at 150 °C and 200 °C remains stable, washing with solvent is expected to have little gain. Indeed, the advancing contact angle after 800 h is 70°±3° and 70°±3°, respectively, similar to the non-washed samples. To confirm that this gain is exclusive to only AP-ALD-coated samples, we carried out an additional experiment by coating the PDMS samples cured at 150 °C with PE-ALD. The advancing contact angle after 800 h is 94°±4°, with the hydrophobic recovery attributed to cracks in the TiO_x coating [31].

Since treated PDMS surfaces may usually not be stored in a nitrogen environment in a glove box, we performed an additional experiment where AP-ALD-coated samples (cured at 70 °C, 150 °C, and 200 °C) were kept in the air at ambient conditions in clean storage. The advancing contact angle after 800 h is 83°±4°, 72°±2°, and 71°±2° respectively, comparable to the samples stored in the nitrogen environment in the glove box. This also shows that both curing at temperature 150 °C and 200 °C and deposition of an (intact) surface-subsurface layer through AP-ALD are essential in obtaining a stable hydrophilic TiO_x coating on PDMS. This stable hydrophilicity, along with a significant percentage of TiO_x on the surface, also indicates a high surface coverage of hydroxyl groups (estimated to be in the order of 10^{14} molecules per cm^2, [43−45]). These hydroxyl groups are of importance for further functionalization.

3.3. Demonstration of functional surface

To demonstrate the ability to functionalize the PDMS surface, we deposit gold nanoparticles (AuNPs) on AP-ALD-coated PDMS samples. Figure 4a shows the presence of AuNPs on the PDMS samples sequentially coated with the Ti and Au precursors (indicated by Au4f signal in Figure 4a, inset), while no appreciable Au4f signal is found on the control PDMS sample coated with only Au precursor that shows no AuNPs (Figure 4b), indicating the importance of hydroxyl groups on the surface of AP-ALD treated layers, in comparison with methyl-dominated bare PDMS [46]. The post-processing of the signal (Suppl. material 1: fig. S5a, calibrated with C1s peak at 248.8eV) shows the presence of mostly Au (0) at the peaks of 84.4eV and 88.1eV, a well-separated spin-orbit component of 3.7eV. From the comparison, the presence of a (stable) TiO_x layer on the PDMS is critical in providing reactive groups for initiating gold-based ALD. Furthermore, to check the purity of the formed AuNPs, an extra scan is conducted on P2p binding energy range as phosphorus is an identifiable element in the ALD Au precursor ligand. Suppl. material 1: fig. S5b shows that the P2p signal is below the detection limit, suggesting the absence of AP-ALD by-products or remaining ligands. We examine the photonic performance of the AuNP-coated sample by measuring the diffuse surface reflectance with UV-Vis. A clear peak of 530 nm is observed (Figure 4c), corresponding to a typical local surface plasmon resonance of AuNPs [47]. We confirm that this peak is not seen in bare PDMS samples and TiO_x-coated PDMS samples. To characterize the particle size distribution, the AuNPs are dispersed by dissolving the underlying TiO_x layer first using HNO_3 1 M, before being washed with ethanol and placed on a TEM grit. The processed image (Figure 4c, inset) shows an average diameter of 4.6 nm and a standard deviation of 0.7 nm accordingly. This AuNP's size with a relatively narrow size distribution is of interest in many applications including photocatalysis and biosensing [48, 49].
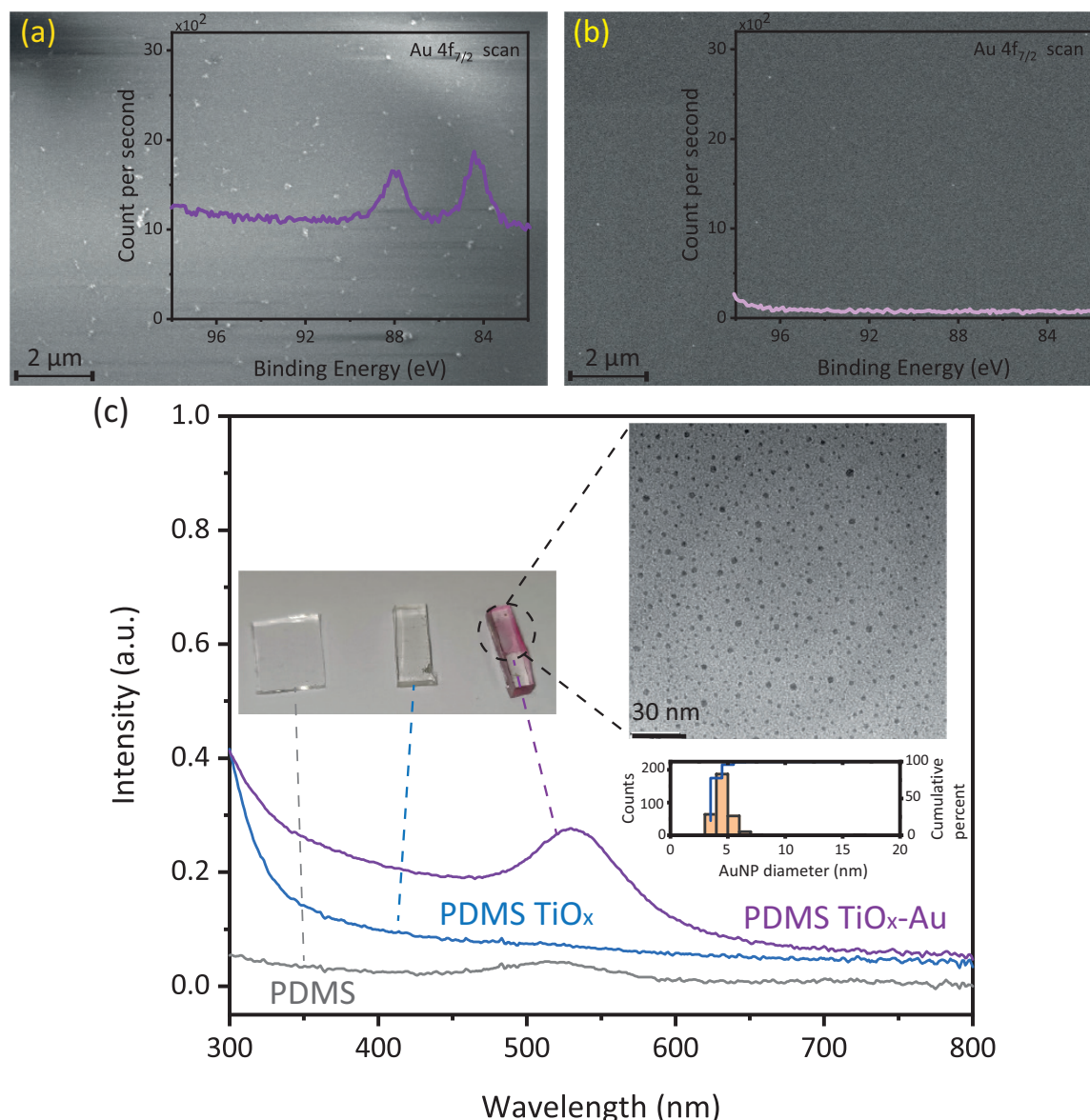
Figure 4. Scanning electron microscopy image of PDMS samples coated with 5 cycles of Au precursors preceded by (**a**) 100 cycles and (**b**) 0 cycles of Ti precursors on PDMS samples cured at 150 °C. Both AP-ALD processes were conducted at 100 °C. The insets show the corresponding XPS spectra at the typical Au4f binding energy range. (**c**) UV-Vis spectra of PDMS, PDMS coated with TiO_x, and PDMS coated with TiO_x and AuNPs. The insets show a photograph of the three samples, a TEM image of the TiO_x-AuNPs-coated PDMS sample, and the corresponding particle size distribution of the AuNPs.

4. Conclusion and outlook

In conclusion, we show that a nano layer of metal oxide can be deposited on the transparent soft elastomer PDMS, providing it with the necessary hydroxyl groups to allow further functionalization of the surface. We find that the surface-subsurface TiO_x layer obtained through atmospheric pressure ALD is critical in providing a surface that remains hydrophilic and stable over prolonged periods of time, with reduced out-diffusion of uncured monomer. For stable hydrophilic TiO_x layers that do not display hydrophobic recovery, curing of PDMS at a temperature of at least 150 °C is found to be of key importance. In comparison with PE-ALD and Th-ALD, AP-ALD offers a robust nano layer that can be further functionalized. We illustrate the further functionalization of the TiO_x-coated PDMS surfaces by depositing gold nanoparticles, also through ALD, opening the opportunity window to high-end applications.

Conflict of interest

Acknowledgments

References

1. K. Raj M and S. Chakraborty, PDMS microfluidics: A mini review, *Journal of Applied Polymer Science* 137, 48958 (2020). https://doi.org/10.1002/app.48958

2. U. Eduok, O. Faye, and J. Szpunar, Recent developments and applications of protective silicone coatings: A review of PDMS functional materials, *Progress in Organic Coatings* 111, 124 (2017). https://doi.org/10.1016/j.porgcoat.2017.05.012

3. I. Miranda, A. Souza, P. Sousa, J. Ribeiro, E. M. Castanheira, R. Lima, and G. Minas, Properties and applications of PDMS for biomedical engineering: A review, *Journal of Functional Biomaterials* 13, 2 (2021). https://doi.org/10.3390/jfb13010002

4. M. P. Wolf, G. B. Salieb-Beugelaar, and P. Hunziker, PDMS with designer functionalities—properties, modifications strategies, and applications, *Progress in Polymer Science* 83, 97 (2018). https://doi.org/10.1016/j.progpolymsci.2018.06.001

5. A. Shakeri, S. Khan, and T. F. Didar, Conventional and emerging strategies for the fabrication and functionalization of PDMS-based microfluidic devices, *Lab on a Chip* 21, 3053 (2021). https://doi.org/10.1039/D1LC00288K

6. B. Gong, J. C. Spagnola, and G. N. Parsons, Hydrophilic mechanical buffer layers and stable hydrophilic finishes on polydimethylsiloxane using combined sequential vapor infiltration and atomic/molecular layer deposition, *Journal of Vacuum Science & Technology A: Vacuum, Surfaces, and Films* 30, 01A156 (2012). https://doi.org/10.1116/1.3670963

7. C. Wang, M. Liu, Z. Wang, S. Li, Y. Deng, and N. He, Point-of-care diagnostics for infectious diseases: From methods to devices, *Nano Today* 37, 101092 (2021). https://doi.org/10.1016/j.nantod.2021.101092

8. F. Akther, S. B. Yakob, N.-T. Nguyen, and H. T. Ta, Surface modification techniques for endothelial cell seeding in PDMS microfluidic devices, *Biosensors* 10, 182 (2020). https://doi.org/10.3390/bios10110182

9. J. Liu, Y. Yao, X. Li, and Z. Zhang, Fabrication of advanced polydimethylsiloxane-based functional materials: Bulk modifications and surface functionalizations, *Chemical Engineering Journal* 408, 127262 (2021). https://doi.org/10.1016/j.cej.2020.127262

10. J. Zhou, D. A. Khodakov, A. V. Ellis, and N. H. Voelcker, Surface modification for PDMS-based microfluidic devices, *Electrophoresis* 33, 89 (2012). https://doi.org/10.1002/elps.201100482

11. Z. Almutairi, C. L. Ren, and L. Simon, Evaluation of polydimethylsiloxane (PDMS) surface modification approaches for microfluidic applications, *Colloids and Surfaces A: Physicochemical and Engineering Aspects* 415, 406 (2012). https://doi.org/10.1016/j.colsurfa.2012.10.008

12. D. Bodas and C. Khan-Malek, Hydrophilization and hydrophobic recovery of PDMS by oxygen plasma and chemical treatment—an sem investigation, *Sensors and Actuators B: Chemical* 123, 368 (2007). https://doi.org/10.1016/j.snb.2006.08.037

13. M. Amerian, M. Amerian, M. Sameti, and E. Seyedjafari, Improvement of PDMS surface biocompatibility is limited by the duration of oxygen plasma treatment, *Journal of Biomedical Materials Research Part A* 107, 2806 (2019). https://doi.org/10.1002/jbm.a.36783

14. S. Hemmilä, J. V. Cauich-Rodríguez, J. Kreutzer, and P. Kallio, Rapid, simple, and cost-effective treatments to achieve long-term hydrophilic PDMS surfaces, *Applied Surface Science* 258, 9864 (2012). https://doi.org/10.1016/j.apsusc.2012.06.044

15. T. Trantidou, Y. Elani, E. Parsons, and O. Ces, Hydrophilic surface modification of PDMS for droplet microfluidics using a simple, quick, and robust method via PVA deposition, *Microsystems & Nanoengineering* 3, 1 (2017). https://doi.org/10.1038/micronano.2016.91

16. G. T. Roman, T. Hlaus, K. J. Bass, T. G. Seelhammer, and C. T. Culbertson, Sol-gel modified poly (dimethylsiloxane) microfluidic devices with high electroosmotic mobilities and hydrophilic channel wall characteristics, *Analytical Chemistry* 77, 1414 (2005). https://doi.org/10.1021/ac048811z

17. J.-B. Orhan, V. Parashar, J. Flueckiger, and M. Gijs, Internal modification of poly (dimethylsiloxane) microchannels with a borosilicate glass coating, *Langmuir* 24, 9154 (2008). https://doi.org/10.1021/la801317x

18. G. T. Roman and C. T. Culbertson, Surface engineering of poly (dimethylsiloxane) microfluidic devices using transition metal sol-gel chemistry, *Langmuir* 22, 4445 (2006). https://doi.org/10.1021/la053085w

19. A. R. Abate, D. Lee, T. Do, C. Holtze, and D. A. Weitz, Glass coating for PDMS microfluidic channels by sol−gel methods, *Lab on a Chip* 8, 516 (2008). https://doi.org/10.1039/b800001h

20. H. Fallahi, J. Zhang, H.-P. Phan, and N.-T. Nguyen, Flexible microfluidics: Fundamentals, recent developments, and applications, *Micromachines* 10, 830 (2019). https://doi.org/10.3390/mi10120830

21. H.-Y. Chen, Y. Elkasabi, and J. Lahann, Surface modification of confined microgeometries via vapor-deposited polymer coatings, *Journal of the American Chemical Society* 128, 374 (2006). https://doi.org/10.1021/ja057082h

22. J. C. Spagnola, B. Gong, and G. N. Parsons, Surface texture and wetting stability of polydimethylsiloxane coated with aluminum oxide at low temperature by atomic layer deposition, *Journal of Vacuum Science & Technology A: Vacuum, Surfaces, and Films* 28, 1330 (2010). https://doi.org/10.1116/1.3488604

23. R. Pessoa, V. dos Santos, S. Cardoso, A. Doria, F. Figueira, B. Rodrigues, G. Testoni, M. Fraga, F. Marciano, A. Lobo, *et al.*, TiO_2 coatings via atomic layer deposition on polyurethane and polydimethylsiloxane substrates: Properties and effects on C. albicans growth and inactivation process, *Applied Surface Science* 422, 73 (2017). https://doi.org/10.1016/j.apsusc.2017.05.254

24. E. Y. Choi, J.-H. Kim, B.-J. Kim, J. H. Jang, J. Kim, and N. Park, Development of moisture-proof polydimethylsiloxane/aluminum oxide film and stability improvement of perovskite solar cells using the film, *RSC Advances* 9, 11737 (2019). https://doi.org/10.1039/C9RA01107B

25. S. Hoshian, V. Jokinen, and S. Franssila, Robust hybrid elastomer/metal-oxide superhydrophobic surfaces, *Soft Matter* 12, 6526 (2016). https://doi.org/10.1039/C6SM01095D

26. S. H. Astaneh, G. Jursich, C. Sukotjo, and C. G. Takoudis, Surface and subsurface film growth of titanium dioxide on polydimethylsiloxane by atomic layer deposition, *Applied Surface Science* 493, 779 (2019). https://doi.org/10.1016/j.apsusc.2019.07.029

27. H. Van Bui, F. Grillo, and J. Van Ommen, Atomic and molecular layer deposition: off the beaten track, *Chemical Communications* 53, 45 (2017). https://doi.org/10.1039/C6CC05568K

28. I. Weisbord, N. Shomrat, R. Azoulay, A. Kaushansky, and T. Segal-Peretz, Understanding and controlling polymer−organometallic precursor interactions in sequential infiltration synthesis, *Chemistry of Materials* 32, 4499 (2020). https://doi.org/10.1021/acs.chemmater.0c00026

29. E. K. McGuinness, F. Zhang, Y. Ma, R. P. Lively, and M. D. Losego, Vapor phase infiltration of metal oxides into nanoporous polymers for organic solvent separation membranes, *Chemistry of Materials* 31, 5509 (2019). https://doi.org/10.1021/acs.chemmater.9b01141

30. T. D. Pinson, Jean, Surface modification of polymers - methods and applications, (John Wiley & Sons, 2020) Chap. 5 *Atomic Layer Deposition and Vapor Phase Infiltration*, pp. 135–157. https://doi.org/10.1002/9783527819249.ch5

31. A. Santoso, A. Damen, J. R. van Ommen, and V. van Steijn, Atmospheric pressure atomic layer deposition to increase organic solvent resistance of PDMS, *Chemical Communications* 58, 10805 (2022). https://doi.org/10.1039/D2CC02402K

32. X. Kang, S. Liu, Z. Dai, Y. He, X. Song, and Z. Tan, Titanium dioxide: from engineering to applications, *Catalysts* 9, 191 (2019). https://doi.org/10.3390/catal9020191

33. X. Liu, P. K. Chu, and C. Ding, Surface modification of titanium, titanium alloys, and related materials for biomedical applications, *Materials Science and Engineering: R: Reports* 47, 49 (2004). https://doi.org/10.1016/j.mser.2004.11.001

34. M. B. Griffiths, P. J. Pallister, D. J. Mandia, and S. T. Barry, Atomic layer deposition of gold metal, *Chemistry of Materials* 28, 44 (2016). https://doi.org/10.1021/acs.chemmater.5b04562

35. F. S. Hashemi, F. Grillo, V. R. Ravikumar, D. Benz, A. Shekhar, M. B. Griffiths, S. T. Barry, and J. R. Van Ommen, Thermal atomic layer deposition of gold nanoparticles: controlled growth and size selection for photocatalysis, *Nanoscale* 12, 9005 (2020). https://doi.org/10.1039/D0NR01092H

36. J. González-Rivera, R. Iglio, G. Barillaro, C. Duce, and M. R. Tinè, Structural and thermoanalytical characterization of 3D porous PDMS foam materials: the effect of impurities derived from a sugar templating process, *Polymers* 10, 616 (2018). https://doi.org/10.3390/polym10060616

37. D. Zhu, S. Handschuh-Wang, and X. Zhou, Recent progress in fabrication and application of polydimethylsiloxane sponges, *Journal of Materials Chemistry A* 5, 16467 (2017). https://doi.org/10.1039/C7TA04577H

38. A. Mata, A. J. Fleischman, and S. Roy, Characterization of polydimethylsiloxane (PDMS) properties for biomedical micro/nanosystems, *Biomedical microdevices* 7, 281 (2005). https://doi.org/10.1007/s10544-005-6070-2

39. R. Seghir and S. Arscott, Extended PDMS stiffness range for flexible systems, *Sensors and Actuators A: Physical* 230, 33 (2015). https://doi.org/10.1016/j.sna.2015.04.011

40. K. Berean, J. Z. Ou, M. Nour, K. Latham, C. McSweeney, D. Paull, A. Halim, S. Kentish, C. M. Doherty, A. J. Hill, *et al.*, The effect of crosslinking temperature on the permeability of PDMS membranes: Evidence of extraordinary CO_2 and CH_4 gas permeation, *Separation and Purification Technology* 122, 96 (2014). https://doi.org/10.1016/j.seppur.2013.11.006

41. D. T. Eddington, J. P. Puccinelli, and D. J. Beebe, Thermal aging and reduced hydrophobic recovery of polydimethylsiloxane, *Sensors and Actuators B: Chemical* 114, 170 (2006). https://doi.org/10.1016/j.snb.2005.04.037

42. K. J. Regehr, M. Domenech, J. T. Koepsel, K. C. Carver, S. J. Ellison-Zelski, W. L. Murphy, L. A. Schuler, E. T. Alarid, and D. J. Beebe, Biological implications of polydimethylsiloxane-based microfluidic cell culture, *Lab on a Chip* 9, 2132 (2009). https://doi.org/10.1039/b903043c

43. A. Boonstra and C. Mutsaers, Relation between the photoadsorption of oxygen and the number of hydroxyl groups on a titanium dioxide surface, *The Journal of Physical Chemistry* 79, 1694 (1975). https://doi.org/10.1021/j100583a017

44. K. Liu, M. Cao, A. Fujishima, and L. Jiang, Bio-inspired titanium dioxide materials with special wettability and their applications, *Chemical Reviews* 114, 10044 (2014). https://doi.org/10.1021/cr4006796

45. E. Hyde and M. Beck, Comprehensive dft study of hydroxyl coverage on titania surfaces, *Applied Surface Science* 498, 143893 (2019). https://doi.org/10.1016/j.apsusc.2019.143893

46. A. Gökaltun, Y. B. Kang, M. L. Yarmush, O. B. Usta, and A. Asatekin, Simple surface modification of poly (dimethylsiloxane) via surface segregating smart polymers for biomicrofluidics, *Scientific Reports* 9, 7377 (2019). https://doi.org/10.1038/s41598-019-43625-5

47. S. Y. Lee, D. Kang, S. Jeong, H. T. Do, and J. H. Kim, Photocatalytic degradation of rhodamine b dye by TiO_2 and gold nanoparticles supported on a floating porous polydimethylsiloxane sponge under ultraviolet and visible light irradiation, *ACS Omega* 5, 4233 (2020). https://doi.org/10.1021/acsomega.9b04127

48. S. Witzel, A. S. K. Hashmi, and J. Xie, Light in gold catalysis, *Chemical Reviews* 121, 8868 (2021). https://doi.org/10.1021/acs.chemrev.0c00841

49. P. Si, N. Razmi, O. Nur, S. Solanki, C. M. Pandey, R. K. Gupta, B. D. Malhotra, M. Willander, and A. de la Zerda, Gold nanomaterials for optical biosensing and bioimaging, *Nanoscale Advances* 3, 2679 (2021). https://doi.org/10.1039/D0NA00961J

E-mail and ORCID

Albert Santoso (a.santoso@tudelft.nl), ORCID: https://orcid.org/0000-0002-6713-5044
Bart J. van den Berg (bart.vdberg@outlook.com)
Saeed Saedy (s.saedy@tudelft.nl), ORCID: https://orcid.org/0000-0003-3822-4678
Eden Goodwin (edengoodwin@cmail.carleton.ca), ORCID: https://orcid.org/0000-0001-5680-468X

Volkert van Steijn ⊙ (v.vansteijn@tudelft.nl), ORCID: https://orcid.org/0000-0002-3322-7004
J. Ruud van Ommen ⊙ (Corresponding author, j.r.vanommen@tudelft.nl), ORCID: https://orcid.org/0000-0001-7884-0323

Supplementary material 1

Supplementary images

Authors: Albert Santoso, Bart J. van den Berg, Saeed Saedy, Eden Goodwin, Volkert van Steijn, J. Ruud van Ommen
Data type: figures (PDF file)
Explanation note: fig. S1: Measurement of the advancing (left) and receding contact angle (right) on AP-ALD-treated PDMS samples. In the main manuscript, we report the advancing contact angles. **fig. S2:** (a) Approximated TiO_x layer thickness obtained from XPS depth profiling with the etch rate determined using a TiO_x layer on a silicon wafer as described previously [31]. (b) XPS depth profiling of AP-ALD coated PDMS samples for 30, 50, 75, and 100 cycles. All PDMS samples are cured at 150 °C. **fig. S3:** Scanning electron microscopy images of AP-ALD treated PDMS samples after 800 h. Both of the left images were cured at 70 °C (the bottom image was washed in cyclohexane before AP-ALD treatment), and the right images were cured at 150 °C (top), and 200 °C (bottom). **fig. S4:** (a) Advancing contact angle measurement on bare PDMS and PDMS coated with PE-ALD, Th-ALD, and AP-ALD. AP-ALD is also performed on washed samples. All PDMS samples were cured at 70 °C. (b) Corresponding XPS surface spectra of the ALD-coated PDMS samples. The XPS spectra show a high presence of Si2p peak and a low presence of Ti2p peak on Th-ALD samples, indicating minimum TiO_x surface coverage. The PE-ALD and AP-ALD samples show the opposite, indicating high TiO_x surface coverage. **fig. S5:** XPS spectrum of (a) Au4f, (b) P2p of coated PDMS samples. The samples were coated with 100 cycles of Ti precursors and 5 cycles of Au precursors. The horizontal line gives the baseline for the background signal. No clear peak of P2p was observed at the measured binding energy range.
Link: https://doi.org/10.15212/aldj.1.105146.suppl1